



Piotr Czarnocki <sup>1</sup>, Tomasz Zagrajek <sup>1</sup>

## Growth stability analysis of embedded delaminations with the use of FE node relocation procedure and effective resistance curve concept

Embedded delamination growth stability was analysed with the help of the FEM combined with a specially developed procedure for node relocation to obtain a smooth variation of the SERR components along the delamination contour. The procedure consisted in the replacement of the actual material with the very compliant fictitious one and the displacement of the delamination front nodes by the previously determined distance in a local coordinate system. Due to this loading, the new delamination front was created. Subsequently, the original material was restored. Evolution under in-plane compression of three initially circular delaminations of diameters  $d = 30, 40$  and  $50$  mm embedded in thin laminates of two different stacking sequences, i.e.,  $0_4//0_{24}^{\circ}$  and  $0_4//90_{20}^{\circ}/0_4^{\circ}$  were considered. It was found that the growth history and the magnitude of the load that triggers unstable delamination growth depended mainly on the combined effects of the initial delamination size, delamination contour, out of plane post-buckling geometry of the disbanded layers, reinforcement arrangement, and magnitude and variation of the SERR components along the delamination contour. To present the combined effect of these features, an original concept of the effective resistance curve,  $G_{Reff}$ , was introduced.

### 1. Introduction

Once a delamination has been detected, then a question arises whether the defected structure could be allowed for service or it should be repaired or even scrapped. The answer can depend on the delamination location, size, and the damage tolerance philosophy adopted for the product in question. Often, no defect growth or slow defect growth approach is applied, (e.g., in the case of airframes)

✉ Piotr Czarnocki, e-mail: [pecz@meil.pw.edu.pl](mailto:pecz@meil.pw.edu.pl)

<sup>1</sup>Institute of Aeronautics and Applied Mechanics, Warsaw University of Technology, Poland.



and delamination growth under cyclic loading must be considered, however, the first question to answer is whether the delamination under consideration would grow under the expected static load and, if so, would this growth be stable or not. In spite of the relevance of these issues, the number of papers accessible in the open literature addressing them is scant.

Delaminations can be due to faulty manufacturing process. Mainly, such flaws result from the air entrapped between reinforcement layers and often they assume almost circular or elliptical shape [1]. Such disbonds will be referred to herein as initial delaminations. It is broadly accepted that delaminations can be treated as interlaminar cracks and, as such, they can be investigated with the help of the Linear Fracture Mechanics or/and the Damage Mechanics [2]. The first step in the assessment of the delamination severity and the threat to the structural integrity the delamination can produce is the determination of the critical external load causing buckling of the thinner of the disbonded layers or both of them, and next, determination of the Strain Energy Release Rate (SERR) values along the delamination front in the post-buckling delamination stage. The problem is not new and attempts to solve it were undertaken more than 30 years ago, however, not until sufficient development of the FEM was achieved, and contact modelling, splitting of nodes and remeshing became possible, was an efficient tool for solving the aforementioned problem available. The early 2D models ([3–6]) represented laminates with through-the-width delaminations. Some of these models offered closed-form solutions [5, 6], easy for application, however, because of the considered delamination geometry, their practical applications were rather modest.

Three-dimensional models having a more practical application were developed with the help of the FEM in combination with the tools offered by the Linear Elastic Fracture Mechanics, i.e., the Virtual Crack Closure Integral (VCCI) concept [7], and the Modified Virtual Crack Closure Integral (MVCCI) concept [8], or the tool offered by the Damage Mechanics i.e., cohesive elements [9]. Due to these combinations, FE models represented more common delaminations such as embedded ones were developed. Early models were only capable of determining variation of the SERR components along the delamination front [10, 11]. These models neither accounted for delamination growth nor were useful for analysing delamination growth stability.

In the more advanced models, to facilitate simulation of delamination growth, special means of coupling the opposite element nodes belonging to the layers undergoing separation were developed, while the laminate layers themselves were modelled with brick elements, e.g., [12–15], or shell elements [9, 16–18]. The specificity of the node coupling consisted in that, if a chosen fracture criterion was met, the ties were removed and then the delamination grew. The nodes could be coupled in various ways: with the help of springs, [13, 14], of *Multi-Point Constraints* (MPC) [16, 19] or with the help of contact elements, [18, 20]. Application of the MVCCI method, (often the VCCT term is used as a synonym for the MVCCI), involves two assumptions, i.e., that the delamination growth is self-similar and that

a delamination already exists. Violation of the former may result in overestimating the SERR values. To avoid this, some correction factors could be used, [16]. The limitation resulting from the need for initial delamination could be removed by application of the Damage Mechanics and use of cohesive elements that could be placed at the interface of the layers expected to undergo delamination [9]. Alternatively, an initial delamination could be formed in the region in which a certain strength criterion regarding interlaminar stress state was met, as indicated by the preceding initial FE analysis [19].

The method to calculate the virtual area to be closed presented in [15], required the finite elements crossing the delamination front to be hexagonal and of the same size. These requirements limited application of such models to straight edge delaminations. This limitation was removed by the method of calculating the virtual area to be closed, presented in [12]. It allowed for modelling growth of circular or elliptical delamination with the use of a mesh of not even elements surrounding the delamination front. The only restriction was that the element sides crossed by the delamination front had to be flat. Advanced, more complete approach for simulating delamination growth than heretofore mentioned is presented in [17]. It combines several earlier concepts [14, 15, 21, 22], allowing for the elimination of important shortcomings pointed out in [21], typical for a standard VCCT, such as, sensitivity of the results to the size of elements at the delamination front, sensitivity to the load step sizes, and prediction of exaggerated values of the SERR components at the corners of zig-zag delamination front. It was shown in [17] that due to specific subroutine proposed in [21], it was possible to eliminate sensitivity of the results to the element size at the delamination front and to the load step size. To eliminate the prediction of exaggerated values of the SERR components, an advantage was taken of the concept presented in [23], which consisted in the calculation of the SERR over a segment of delamination front located between the two nodes for which exaggerated SERR values were expected rather than at those nodes themselves. In the case of not smooth delamination front heaving corners or/and different size elements across the front, there appears the problem of how to define the area and the distance over which it must be virtually closed, and how to define the closing force needed for calculation of the SERR components. One possible solution to this problem, adopted in [17], is presented in [14, 15, 22]. Another procedure being a modification of that in [14, 15, 22] is described in [23, 24]. Their authors showed that it allowed for more precise determination of the aforementioned quantities. Aforementioned models are non-linear. It results in a relatively high computational cost. In case of preliminary damage tolerance considerations, this cost can be reduced by the application of a specific methodology, presented in [25]. This methodology is based on a linear buckling analysis of the delamination under consideration and the global variation in potential energy associated with a small delamination growth. With the use of this method, the critical fracture load and the location of the delamination propagation origin can be determined, however, application of this method is limited to delaminations the growth of which can

be mainly attributed to Mode I fracture and the remaining fracture modes can be neglected.

In this paper, growth and growth stability of embedded delaminations resulting from manufacturing imperfections, such as air pockets are considered. Contours of such delaminations are closed curves and often can be well approximated with circles or ellipses. Unlike in the case of simple delamination tests, e.g., DCB test, they do not propagate in a self-similar manner. The observed variation in delamination resistance can be due not only to the development of a damage zone in front of delamination, as it is the case in the DCB test. It will be shown that, in the case of embedded delaminations, their resistance against growth also depends on their contours, on out of plane post-buckling geometry of the disbanded layers, on the reinforcement arrangement, and on the magnitude and variation of the SERR components along a delamination contour. These features interact with each other and for this reason it would be very difficult to analyse separately the ways they affect delamination growth. Therefore, only combined effect of these features on the delamination process will be shown. To present it, an original concept of the effective resistance curve,  $G_{Reff}$ , was introduced. Delamination growth produces a release of a certain amount of the strain energy, which is equated with the energy needed for the formation of the new delamination surface. Herein, this energy was named the Effective Resistance Against Delamination Growth and denoted  $G_{Reff}$ . The presented investigations consisted in the simulation of the growth history of three delaminations differing by initial diameters. The delaminations were embedded in hypothetic laminates of two different reinforcement arrangements and it was assumed that the layers forming the laminate were of sufficient strength to assure the absence of intralaminar failure.

Altogether, six defected laminar structures were considered, as shown in Table 1.

Table 1.

Matrix of numerical simulations

Laminate number	Reinforcement arrangement ("//" indicates a location of delamination)	Delamination diameter [mm]		
		30	40	50
1	$0_4^{\circ} // 0_{24}^{\circ}$	30	40	50
2	$0_4^{\circ} // 90_{20}^{\circ} // 0_4^{\circ}$	30	40	50

In the quoted delamination growth modelling procedures, the region of the expected delamination growth was meshed with brick elements of possible similar dimensions. It was shown that, with the use of such elements, it is possible to reproduce initially smooth delamination front. However, as delamination grows its contour undergoes reshaping and becomes polyline with several approximately  $90^{\circ}$  corners at nodes. This, in turn, results in zig-zag variation of the SERR components along the newly created delamination front, e.g., [24].

The authors of this paper took advantage of the virtual crack closure integral concept (not the MVCCI one), in combination with the specific node relocation procedure. A typical remeshing usually involves the generation of new nodes. The proposed procedure eliminated this need: the original mesh was modified by the gradual relocation of the nodes if the assumed delamination criterion had been met. This procedure will be described in more detail in section 2.3. Due to such node relocation, the contour of the delamination remained smooth throughout the whole process of the delamination growth simulation and the SERR values varied smoothly from node to node. The concept of node relocation to mimic delamination front movement had been already applied in [26], but the procedure of node relocation itself, presented in this work, was original.

## 2. Delamination growth modelling

### 2.1. Delamination growth criterion

To ascertain that a growth of delamination takes place, the determined SERR values must be compared against suitable delamination criterion. It should be kept in mind that the available delamination criteria e.g., [27–33], are phenomenological. They were obtained by curve fitting of the experimental data related to a particular laminate, and for this reason these criteria are not universal. Furthermore, they account for the presence of just two fracture modes. Since, in the case of embedded delaminations all three components of the SERR are present and they are of the same magnitude, the suitable criterion must account for all of them. Unfortunately, the phenomenological criteria that take into consideration all three fracture modes are not available. The available ones are simple modifications of the aforementioned done by including a component accounting for the remaining fracture mode [34]. Furthermore, they lack experimental validation. As a consequence, the quantitative evaluation of simulation results could be difficult.

For the purpose of the intended simulations, an advantage was taken of a simple delamination criterion given in [34]. With the help of this criterion, the delamination index  $K$  was defined:

$$K = \frac{G_I}{G_{Ic}} + \frac{G_{II}}{G_{IIc}} + \frac{G_{III}}{G_{IIIc}} - 1 \geq 0. \quad (1)$$

It was assumed that the delamination growth takes place if  $K \geq 0$ . Later, in the body of the paper, consequences of applying the alternative delamination index  $K_a$  will be shortly discussed, taking advantage of the more complex delamination criterion proposed also in [34]:

$$K_a = \frac{G_\Sigma}{G_{Ic} + (G_{IIc} - G_{Ic}) \left( \frac{G_{II} + G_{III}}{G_\Sigma} \right)^\eta + (G_{IIIc} - G_{Ic}) \left( \frac{G_{II} + G_{III}}{G_\Sigma} \right)^\eta} - 1 \geq 0, \quad (2)$$

where:  $G_\Sigma = G_I + G_{II} + G_{III}$  and  $\eta$  are curve fitting parameters.

It should be mentioned that despite the fact that  $G_{Ic}$ ,  $G_{IIc}$ ,  $G_{IIIc}$  values depend on the difference in the reinforcement direction across the fracture plane, as well as, on the direction of the delamination propagation relative to the reinforcement direction, these dependencies are ignored in this paper because of the lack of relevant data.

## 2.2. FE model

The assumed mechanical properties of the single layer forming the hypothetical laminates under consideration and the assumed critical values of the SERR for three fracture modes are shown in Table 2.

Table 2.

Assumed mechanical properties

Young's modulus [MPa]			Poisson's ratio			Shear modulus [MPa]			Critical value of the strain energy release rate [N/mm]		
$E_1$	$E_2$	$E_3$	$\nu_{12}$	$\nu_{23}$	$\nu_{31}$	$G_{12}$	$G_{23}$	$G_{31}$	$G_{Ic}$	$G_{IIc}$	$G_{IIIc}$
128 290	8 760	8 760	0.288	0.320	0.288	4 270	3 000	4 270	0.3	0.9	0.9

The geometry of the plate under consideration and FE mesh in the vicinity of the delamination front are sketched in Fig. 1. The nominal plate dimensions were as follows: length,  $l = 150$  mm, width,  $s = 100$  mm and thickness  $t = 4$  mm. It contained an embedded initially circular delamination, located in the plate centre. For all the considered models, (Table 1), a single reinforcement layer (prepreg) was 0.142 mm thick. The debonded sub-laminate (delamination) was composed of four such prepreg layers and was 0.568 mm thick. The substrate was composed of 24 layers and was 3.432 mm thick. The FE simulation of the delamination growth was carried out with the use of ANSYS v.15 FE code and with the help

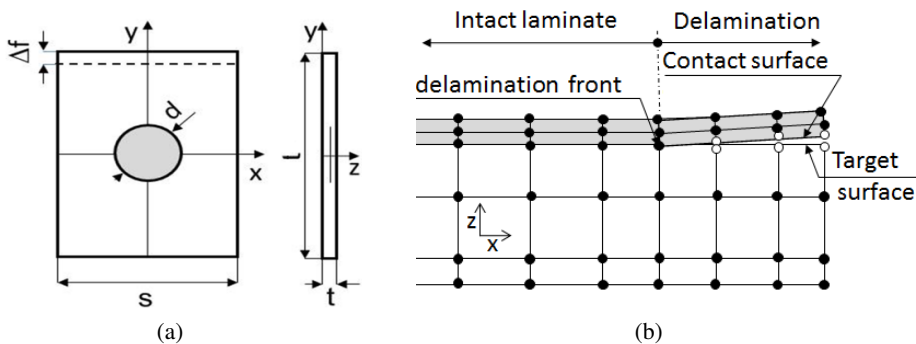


Fig. 1. Geometry of the defected plate: (a) the  $\Delta f$  and dashed line represent displacement of the plate edge due to the prescribed loading, and (b) the FE mesh in the vicinity of the delamination front at plane  $y = 0$ . The substrate is not shadowed

of the original node relocation procedure explained in the next subchapter. The laminate was modelled with eight node SOLID185, (Layered Structural Solid (KEYOPT(3) = 1), elements. The delamination and substrate were represented by two and three layers of such elements, respectively, Fig. 1. To prevent penetration, surface-to-surface ANSYS contact elements (CONTA173 and TARGET170) were used.

The imposed constraints were the following.

$$\text{for } y = \pm \frac{l}{2}, x = \pm \frac{s}{2} \text{ and } z = -\frac{t}{2}, u_z = 0;$$

$$\text{for } y = \frac{l}{2} \text{ and } z = \left(-\frac{t}{2}, \frac{t}{2}\right), u_y = -\Delta f \text{ (external loading);}$$

$$\text{for } y = -\frac{l}{2} \text{ and } z = \left(-\frac{t}{2}, \frac{t}{2}\right), u_y = 0;$$

$$\text{for } y = -\frac{l}{2} \text{ and } x = z = 0, u_x = 0.$$

The simulations were carried out under displacement control: the external loading was increased gradually by the displacement increments,  $\Delta f$ , which were equal to 2.5% of the displacement producing buckling. To determine this value, a preliminary *eigenvalue buckling analysis was performed*. The maximum node shift,  $\delta_{\max}$  was equal to 0.1 mm. For the mesh designed, several try runs had been performed with decreasing  $\delta_{\max}$ . In general, the decrease in  $\delta_{\max}$  smoothed the crack front line and in consequence, the variation in  $G$  values. The adoption of  $\delta_{\max} = 0.1$  resulted from the observation that for  $\delta_{\max} < 0.1$  the running time significantly increased with no substantial improvement on the smoothness of the  $G$  variation along the front line. Examples of the mesh geometry representing the initial delamination and the delamination at the instability threshold are shown in Fig. 2.

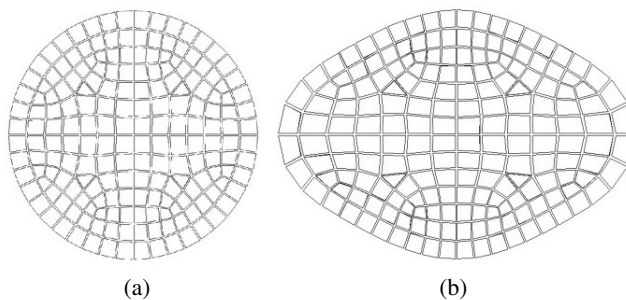


Fig. 2. Example of the meshes representing geometry of the initial delamination (a) and at the instability threshold (b)

It was assumed that the fracture mode partition can appropriately be done with the use of the following equations

$$G_I = \frac{\frac{1}{2}P_z\Delta u_z}{2S_{b'c'd'dcb}}, \quad (3a)$$

$$G_{II} = \frac{\frac{1}{2}P_y\Delta u_y}{2S_{b'c'd'dcb}}, \quad (3b)$$

$$G_{III} = \frac{\frac{1}{2}P_x\Delta u_x}{2S_{b'c'd'dcb}}. \quad (3c)$$

This is a common approach, e.g., [35, 36], nevertheless, the authors are aware that some other approaches exist [37], however, they refer to very local stress state and assume homogeneity of material which is not the case as far as polymer composites reinforced with continuous fibres are considered.

### 2.3. Node relocation procedure

The relocation procedure consisted of several steps. At the beginning, local Cartesian coordinate systems were assigned to all the nodes located at the delamination front. To define each of the local coordinate systems, three **neighbouring** nodes were used, e.g., a, c and e, (c – middle node, and a and e – external nodes) as shown in Fig. 3. A local  $x$ -axis was defined first based on the requirement that it must pass through the external nodes, a and e. Next, the  $y$ -axis was defined based on the requirement that this axis should pass through the middle node c and be perpendicular to the already defined  $x$ -axis. To accomplish this, a series of the following ANSYS commands was issued in the following order: CS, WPCSYS, NWPAVE and CSWPLA.

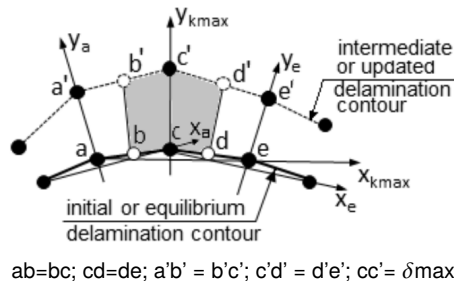


Fig. 3. Local coordinate systems used for the node relocation.

Coordinate systems  $y_a-x_a$ ,  $y_{kmax}-x_{kmax}$ , and  $y_e-x_e$  are associated with nodes a, c and e, respectively. The shadowed area is associated with the nodal forces at node c



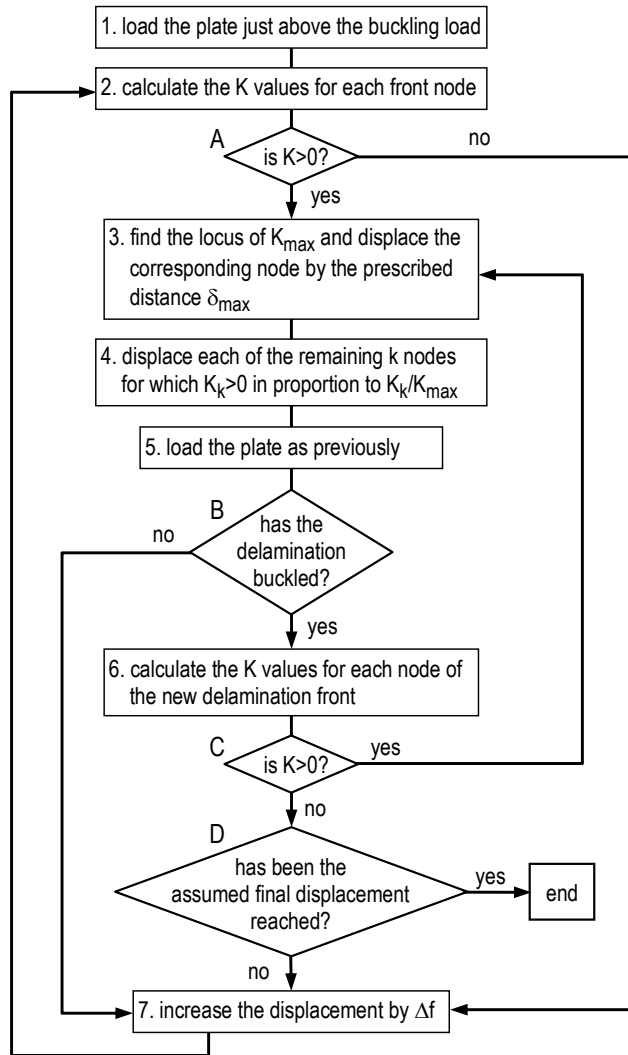


Fig. 4. Procedure used to simulate growth of delamination

Next, the first five steps of the flowchart, Fig. 4, were completed as follows. Just after exceeding the buckling load, the  $K$  values were evaluated for each node located at the delamination front. If the criterion (1) was not met for any of the considered nodes, the external load was increased by the prescribed displacement increment,  $\Delta f$ , and the procedure was repeated. If the opposite was true, in-plane displacements of the nodes at the delamination front were read and stored. Then, the actual material was replaced with the fictitious homogeneous one, designed in this way that its modulus was decreasing with the increasing distance from the delamination front, as shown in Fig. 5.

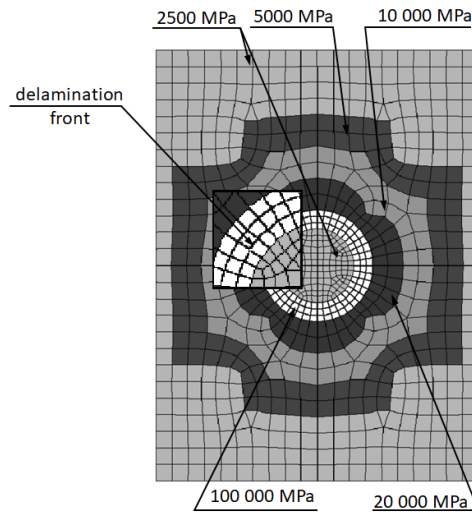


Fig. 5. Fictitious material definition. Its modulus was decreasing incrementally with the increasing distance from the delamination front, as indicated by the numerical values. Each gray level represents material of one modulus value

Next, the node of the highest  $K$  value was displaced in the local  $y$ -direction by the prescribed distance,  $\delta_{\max}$ , e.g., node  $c$  to position  $c'$ , as shown in Fig. 3. The remaining  $n$  nodes, for which  $K_n$  met the condition

$$K_{\max} > K_n > 1, \quad (4)$$

were displaced in the corresponding local  $y_n$  directions by the distance  $\delta_n$ , calculated according to:

$$\delta_n = \delta_{\max} \frac{K_n}{K_{\max}}. \quad (5)$$

Due to this loading, the new delamination front was created. The locations of all the remaining nodes were shifted accordingly due to the deformation of the fictitious material. This way all these nodes assumed new positions. Next, the original material was restored and the 5th step of the flowchart was completed.

As a result of this process, the new delamination geometry was created, for which the new set of  $K$  values was calculated for all the nodes at the new delamination front. The graph in Fig. 6 provides additional explanation. Points  $P_1$  and  $P_2$  represent the scenario in which condition D (procedure in Fig. 4) was reached just in one loop, while points  $P_3$ ,  $P_3^I$ ,  $P_3^{II}$  and  $P_4$  represent the scenario in which condition C was answered “yes” two times in row and two loops were needed to reach condition D. Points  $P_1$ – $P_7$  represent stable delamination growth while point  $P_9$  and the consecutive points correspond to unstable growth.

The  $G_I$ ,  $G_{II}$  and  $G_{III}$  components in (1) were calculated with the help of the virtual crack closure concept. However, to avoid possible problems resulting

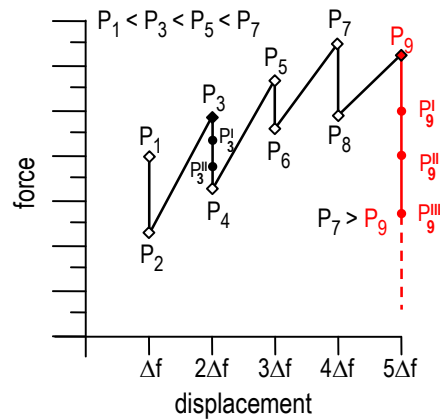


Fig. 6. Load variation in the course of delamination growth

from the violation of assumptions concerning a self-similar delamination growth, pointed out in [16], the MVCCI presented in [8], was not applied. The node opening and nodal forces to close it were calculated for the same pair of nodes, (i.e., a dual FE calculation was involved: (a) for the pair of nodes under consideration nodal forces were determined, next, (b) the nodes were disconnected and the relative displacement of the disconnected nodes was determined). It was assumed that the  $G_I$ ,  $G_{II}$  and  $G_{III}$  components were equal to the half of the product of the nodal displacements and the corresponding forces divided by the doubled shadowed area, as shown in Fig. 3.

#### 2.4. Construction of $G_{\text{Reff}}$ curve

The coordinates of each point of this curve were determined as follows. With the help of the described node relocation procedure, the new delamination contour and the corresponding new delamination area,  $A_n$ , were defined for each displacement increment,  $\Delta f_n$ . The corresponding delamination area increment,  $\Delta A_n$ , was calculated by subtracting the consecutive delamination areas, i.e.,

$$\Delta A_n = A_n - A_{n-1}. \quad (6)$$

The SERR value,  $G_{Rn}$ , needed for the creation of the new surface  $2\Delta A$  was calculated according to the following equation:

$$G_{Rn} = \frac{\Delta E_{el}}{2\Delta A}, \quad (7)$$

where:  $\Delta E_{el}$  – change in the elastic energy taking place in the course of creation of the new surface  $2\Delta A$ , calculated based on the element stress and strain, (with the help of ETABLE ANSYS command).

### 3. Results

The results will be discussed in terms of changes in delamination contours, changes in the distribution of the SERR component values and the  $K$  values along the delamination front, and in terms of the delamination growth stability.

The delamination contours for both the laminates for the instability thresholds are shown in Fig. 7. The initial delamination contours, (just after buckling of delamination), are shown with dashed lines. It could be noticed that all delaminations were growing, essentially, in the transverse direction relative to the direction of loading. Only for the smallest delaminations, some growth in the direction parallel to the loading direction occurred, but it was much smaller than that in the transverse direction. This finding indicated that 2D models are not applicable for analysing embedded delaminations, even if they are significantly elongated in the direction transverse to loading, since 2D models represent delaminations that propagate only in the direction parallel to the loading.

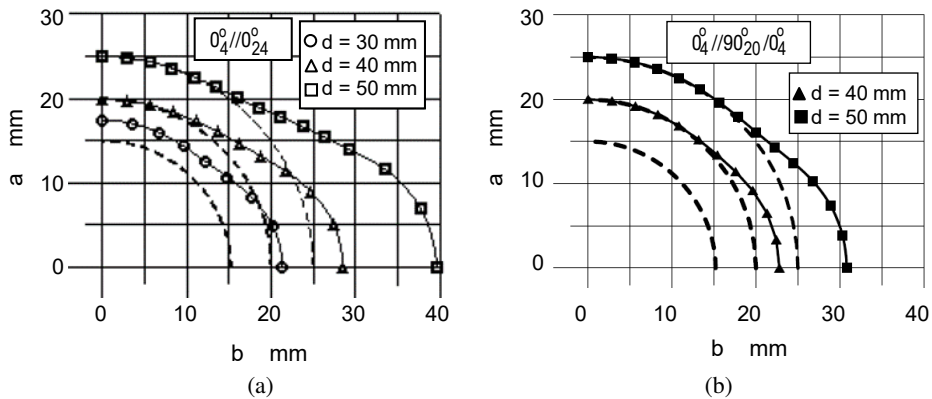


Fig. 7. Delamination contours corresponding to the instability thresholds for laminate  $0_4^0//0_{24}^0$  (a) and laminate  $0_4^0//90_{20}^0//0_4^0$  (b). Notice that for the delamination of  $d = 30$  mm embedded in the latter the stable growth did not occur, therefore for this delamination the contour corresponding to the instability threshold is not shown

It could also be noticed that all the delaminations embedded in the  $0_4^0//0_{24}^0$  laminate were more elongated at the instability threshold than that embedded in the  $0_4^0//90_{20}^0//0_4^0$  one.

Predominate growth of the delaminations in the transverse direction was reflected by the variation of the  $K$  values with the normalised length of the delamination front,  $s$ , Figs. 8 and 9. The shown SERR components were normalised with respect to the maximum value of  $G_{\Sigma}$ . The values of the  $s$ -coordinate were calculated as the ratio between the actual distance from the positive  $y$ -axis measured clockwise along the delamination front and the total delamination front length. The  $G_I$ ,  $G_{II}$ ,  $G_{III}$ ,  $G_{\Sigma}$  and  $K$  values varied periodically with  $s$ , (with periods  $s/2$ ), and for the sake of clarity they are shown in the range  $0-s/2$ , only.

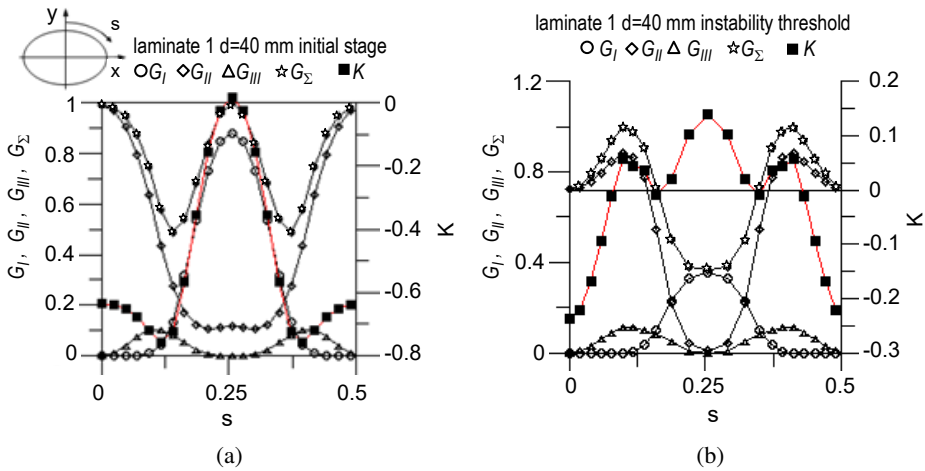


Fig. 8. Variation of the SERR components and delamination index with  $s$  coordinate for the initial stage (a) and the at instability threshold for delaminations embedded in  $0_4^{\circ}/0_{24}^{\circ}$  laminate (b)

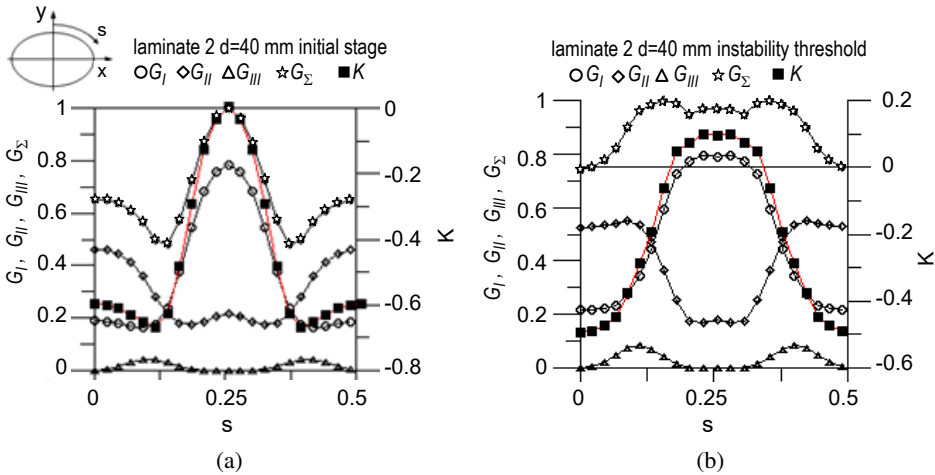


Fig. 9. Variation of the SERR components and delamination index with  $s$  coordinate for the initial stage (a) and the at instability threshold for delaminations embedded in  $0_4^{\circ}/90_{20}^{\circ}/0_4^{\circ}$  laminate (b)

Initially, the values of  $K = K_{\max}$  and  $G_\Sigma = G_{\Sigma \max}$  were located at  $s = 0.25$ , however, the changes in the delamination contours produced relocation of the  $G_{\Sigma \max}$ , while the location of  $K_{\max}$  did not change, (compare corresponding plots in Fig. 8 and in Fig. 9), therefore, the most intensive delamination growth did not correspond to the  $G_{\Sigma \max}$ , as it could be expected. Location of  $K_{\max}$  could also be affected by the choice of delamination criterion and by the mutual relations between the critical values of  $G_{Ic}$ ,  $G_{IIc}$  and  $G_{IIIc}$ , Fig. 10. For example, comparing the result yielded by criterion (1) and  $G_{Ic}/G_{IIc} = G_{Ic}/G_{IIIc} = 1/3$  with that yield by criterion (2) and the same ratios of the SERR components we can clearly see

that according to criterion (1) the most intensive delamination growth would occur for  $s = 0.25$  while according to criterion (2) – for  $s \approx 0.2$  and  $s \approx 0.3$ . It could be also noticed that, for example, for criterion (2) and  $G_{Ic}/G_{IIc} = G_{Ic}/G_{IIIc} = 1/3$  most intensive delamination growth would occur for  $s \approx 0.2$  and  $s \approx 0.3$  while for  $G_{Ic}/G_{IIc} = G_{Ic}/G_{IIIc} = 2/5$ , for  $s \approx 0.1$  and  $s \approx 0.4$ .

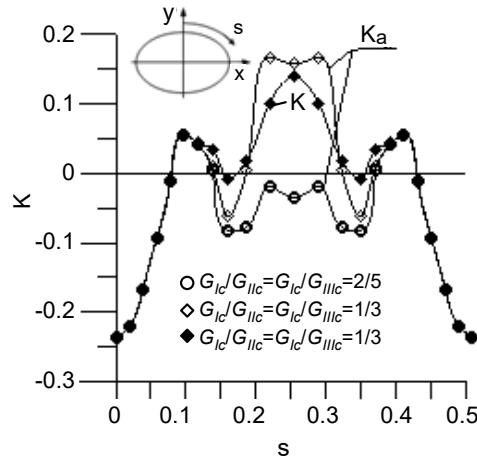


Fig. 10. Variation of delamination indexes  $K$  (◆) and  $K_a$  (○, ◇) with  $s$  co-ordinate

Growth stability of the delaminations under consideration could be assessed by inspection of the relationship between the variation of the delamination area and the external loading expressed in terms of nominal strain,  $\varepsilon = \frac{\Delta f}{l}$ , as shown in Fig. 11. The graphs depict the delamination growth history from the buckling strains to the strains corresponding to the threshold of the unstable delamination growth,  $\varepsilon_{instab}$ .

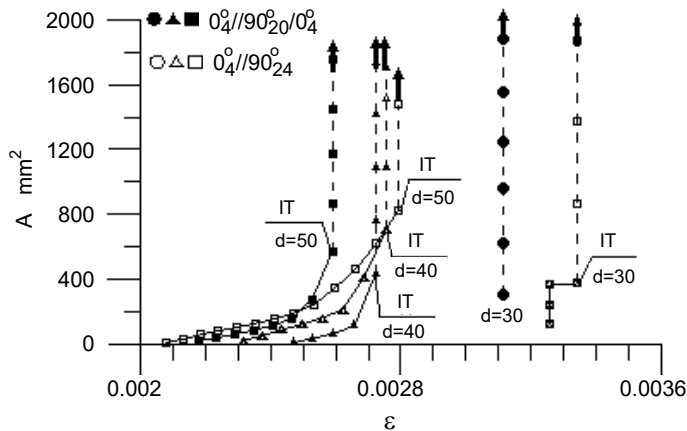


Fig. 11. Growth history of delamination embedded in  $0_4^0//90_{24}^0$  laminate and in  $0_4^0//90_{20}^0//0_4^0$  laminate (closed symbols). Stable growth is shown with continuous lines

The vertical sections of the graphs, shown with dashed lines, correspond to  $\varepsilon = \varepsilon_{\text{instab}}$  and present the unstable delamination growths, since the delamination grew at a constant strain. The energy to produce the new free surface was driven from the elastic energy stored in the system. The symbols beyond the one denoted IT represent some transient unstable stages, while the symbols antecedent IT represent delamination stages for which equilibrium was reached for the given load, and the further growth required a gradual increase in the external load.

The values of  $\varepsilon_{\text{instab}}$  differed depending on the diameters of the initial delaminations and, in general, decreased as the delamination diameters increased. It could also be noticed that the values of  $\varepsilon_{\text{instab}}$  were affected by the layer stacking, (compare graphs with open and closed symbols in Fig. 12). For the delamination of the same initial diameters, the strains corresponding to buckling and instability threshold were lower for the delaminations embedded in the  $0_4^\circ//90_{20}^\circ/0_4^\circ$  laminate than for the ones embedded in the  $0_4^\circ//0_{24}^\circ$  one. It could be attributed to the stronger lateral restraint imposed onto the delaminations embedded in the first laminate due to the lower Poisson ratio of the substrate than that of the substrate of the second one. An interesting feature of the delamination growth history was that small delaminations did not alert or alerted to a lesser degree about approaching unstable growth than the larger ones did. For the smallest delaminations, the unstable growths took place already at the buckling strains, while for the larger ones, to produce the delamination growth, the external load had to be increased. It was a consequence of the difference in the buckling strains, which for smaller delaminations were higher and more elastic energy was available for the delamination growth.

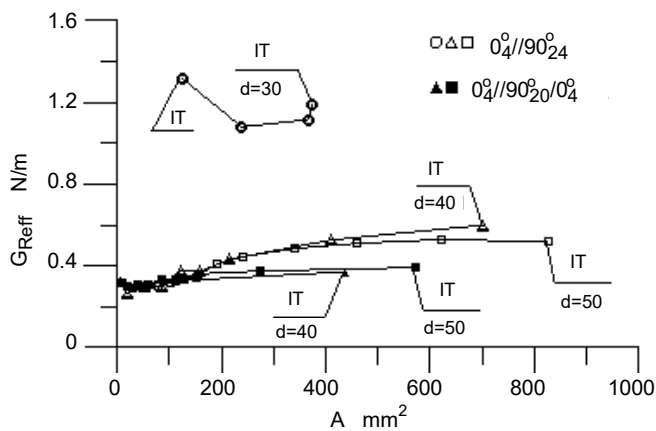


Fig. 12. Effective resistance  $G_{\text{Reff}}$  curves for delamination embedded in  $0_4^\circ//0_{24}^\circ$  laminate (open symbols) and in  $0_4^\circ//90_{20}^\circ/0_4^\circ$

Some qualitative verification of the obtained results can be made by comparing them against the results of the numerical analysis presented in the open literature [23, 38]. However, this comparison is limited to delamination growth

directions. The literature results concerned delaminations at  $0^\circ/90^\circ$  interface of  $[(+45^\circ/-45^\circ/0^\circ/90^\circ)_4]_S$  and  $[0^\circ/90^\circ]_7$  laminates indicated predominant transverse growth of delaminations, as did the results obtained by the authors. To the best of the authors' knowledge, there are no papers in the open literature concerning delamination growth stability of embedded delaminations, so a similar comparison cannot be made. Presently, in the author's opinion, it would be very difficult to carry out quantitative analysis with regard to delamination propagation and propagation stability, as well as, to provide an experimental quantitative verification of the obtained numerical results, at all. There are at least two reasons for that. For the time being, there is a lack of relevant and sufficient data concerning the critical values of the SERR. Albeit, for CF/Epoxy laminates the data on the critical SERR values concerning delamination running at  $0^\circ//0^\circ$  and  $0^\circ//90^\circ$  interfaces are available, unfortunately they pertain mainly to the delaminations running in the direction parallel to the reinforcement. Available data accounting for different propagation directions are scant despite the fact that it has been experimentally proved that such dependency exists and is meaningful [39, 40]. It is clearly visible that the direction of delamination front varies along the delamination contours with respect to the directions of fibres at the potentially created surfaces for all embedded delaminations, and so does the delamination growth direction. This is an important feature and must be taken into consideration if the growth of embedded delaminations is to be quantitatively analysed. The lack of the aforementioned data makes any results of quantitative analysis and its experimental verification unreliable. Unfortunately, the data provided in just mentioned literature are not sufficient. Furthermore, in the case of laminates, there isn't any generally accepted theory available based on which a reliable delamination criterion accounting for all three fracture modes could be established, and experimental results that could be used to construct a phenomenological criterion a phenomenological criterion that accounts for three fracture modes aren't available, so far.

#### 4. Conclusions

Growth and growth stability of initially circular delaminations of three different diameters  $d = 20, 40, 50$  mm embedded in two laminates of stacking sequences  $0_4^\circ//0_{24}^\circ$  and  $0_4^\circ//90_{20}^\circ/0_4^\circ$  were investigated with the help of FE models. To mimic the delamination front evolution, an advantage of the virtual crack closure concept was taken in combination with a specially developed node relocation procedure to obtain a smooth delamination contour, as well as, a smooth variation of the SERR components along it. Since, the applied delamination criterion accounted neither for variation of the critical SERR components with reinforcement configuration, nor for variation of these components with the delamination propagation direction relative to the reinforcement directions, the obtained results clearly exposed the combined effects of delamination contour, out of plane post-buckling geometry of the disbanded layers, reinforcement arrangement, and the magnitude and variation



of the ratios of the SERR components along the delamination contour exerted on the delamination growth. To present the combined effect of these features, an original concept of the effective resistance curve,  $G_{Reff}$ , was introduced. Also, it was shown that the  $G_I$ ,  $G_{II}$ ,  $G_{III}$ ,  $G_{\Sigma} = f(s)$  and  $K = f(s)$  relationships were different for different delamination contours and layer stackings. It was shown that, for larger delaminations, a meaningful increase in the external load above the buckling one was needed to induce the unstable propagation, while the smallest delaminations propagated in an unstable manner just after buckling. It was also clearly visible that the increase in the transverse delamination restraint shifted the instability thresholds to lower external loading, i.e., expedited it. In all the cases under consideration, predominant delamination growth in the direction transverse to the loading direction was observed and only for the smallest delaminations some growth in the direction parallel to the loading was also present. This finding indicated that 2D models are not applicable for analysing embedded delaminations, even if they are significantly elongated in the direction transverse to loading since 2D models represent delaminations that propagate only in the direction parallel to the loading.

Manuscript received by Editorial Board, September 22, 2020;  
final version, November 13, 2020.

## References

- [1] C. Kassapoglou and J. Hammer. Design and analysis of composite structures with manufacturing flaws. *Journal of American Helicopter Society*, 35(4):46–52, 1990. doi: [10.4050/JAHS.35.46](https://doi.org/10.4050/JAHS.35.46).
- [2] R.C. Yu and A. Pandolfi. Modelling of delamination fracture in composites: a review. In: S. Sridharan (ed.), *Delamination Behaviour of Composites*, pages 429–451. Woodhead Publishing Ltd., Cambridge, 2008.
- [3] H. Chai, C.D. Babcock, and W.G. Knauss. One dimensional modelling of failure in laminated plates by delamination buckling. *International Journal of Solids and Structures*, 17(11):1069–1083. 1981.
- [4] J.D. Whitcomb. Finite element analysis of instability related delamination growth. *Journal of Composite Materials*, 15(5):403–426, 1981. doi: [10.1177/002199838101500502](https://doi.org/10.1177/002199838101500502).
- [5] V.V. Bolotin. Defects of the delamination type in composite structures. *Mechanics of Composite Materials*, 20(2):173–188, 1984. doi: [10.1007/BF00610358](https://doi.org/10.1007/BF00610358).
- [6] L.M. Kachanov. *Delamination Buckling of Composite Materials*, pages 57–67, Kuwer Academic Press, 1988.
- [7] G.R. Irwin. *Fracture, Handbook der Physik (Fracture, Handbook of Physics)*, pages 551–590. Springer, Berlin, 1958. (in German).
- [8] E.F. Rybicki and M.F. Kanninen. A finite element calculation of stress intensity factors by a modified crack closure integral. *Engineering Fracture Mechanics*, 9(4):931–938, 1977. doi: [10.1016/0013-7944\(77\)90013-3](https://doi.org/10.1016/0013-7944(77)90013-3).
- [9] C. Bisagni, R. Vescovini, and C.G. Davila. Assessment of the damage tolerance of post-buckled hat-stiffened panels using single-stringer specimens. In: *51st AIAA/ASME/ASCE/AH-S/ASC Structures, Structural Dynamics and Materials Conference*, paper no. AIAA2010-2696, Orlando, USA, 12–15 April, 2010. doi: [10.2514/6.2010-2696](https://doi.org/10.2514/6.2010-2696).

- [10] J.D. Whitcomb. Three-dimensional analysis of a postbuckled embedded delamination. *Journal of Composite Materials*, 23(9):862–889, 1989. doi: [10.1177/002199838902300901](https://doi.org/10.1177/002199838902300901).
- [11] J.D. Whitcomb. Analysis of a laminate with a postbuckled embedded delamination, including contact effect. *Journal of Composite Materials*; 26(10):1523–1535, 1992. doi: [10.1177/002199839202601008](https://doi.org/10.1177/002199839202601008).
- [12] H. Okada, M. Higashi, M. Kikuchi, Y. Fukui, and N. Kumazawa. Three dimensional virtual crack closure-integral method (VCCM) with skewed and non-symmetric mesh arrangement at the crack front. *Engineering Fracture Mechanics*, 72(11):1717–1737, 2005. doi: [10.1016/j.engfracmech.2004.12.005](https://doi.org/10.1016/j.engfracmech.2004.12.005).
- [13] D. Xie and S.B. Biggers Jr. Progressive crack growth analysis using interface element based on the virtual crack closure technique. *Finite Elements in Analysis and Design*, 42(11):977–984, 2006. doi: [10.1016/j.finel.2006.03.007](https://doi.org/10.1016/j.finel.2006.03.007).
- [14] D. Xie and S.B. Biggers Jr. Strain energy release rate calculation for a moving delamination front of arbitrary shape based on the virtual crack closure technique. Part I: Formulation and validation. *Finite Elements in Analysis and Design*, 73(6):771–785, 2006. doi: [10.1016/j.engfracmech.2005.07.013](https://doi.org/10.1016/j.engfracmech.2005.07.013).
- [15] D. Xie and S.B. Biggers Jr. Strain energy release rate calculation for a moving delamination front of arbitrary shape based on the virtual crack closure technique. Part II: Sensitivity study on modeling details. *Finite Elements in Analysis and Design*, 73(6):786–801, 2006. doi: [10.1016/j.engfracmech.2005.07.014](https://doi.org/10.1016/j.engfracmech.2005.07.014).
- [16] A.C. Orifici, R.S. Thomson, R. Egenhardt, C. Bisagni, and J. Bayandor. Development of a finite element analysis methodology for the propagation of delaminations in composite structures. *Mechanics of Composite Materials*, 43(1):9–28, 2007. doi: [10.1007/s11029-007-0002-6](https://doi.org/10.1007/s11029-007-0002-6).
- [17] A. Riccio, A. Raimondo, and F. Scaramuzzino. A robust numerical approach for the simulation of skin–stringer debonding growth in stiffened composite panels under compression. *Composites Part B: Engineering*, 71:131–142, 2015. doi: [10.1016/j.compositesb.2014.11.007](https://doi.org/10.1016/j.compositesb.2014.11.007).
- [18] D. Zou and C. Bisagni. Study of skin-stiffer separation in T-stiffened composite specimens in post-buckling condition. *Journal of Aerospace Engineering*, 31(4), 2018. doi: [10.1061/\(ASCE\)AS.1943-5525.0000849](https://doi.org/10.1061/(ASCE)AS.1943-5525.0000849).
- [19] A.C. Orifici, R.S. Thomson, R. Degenhardt, C. Bisagni, and J. Bayandor. A finite element methodology for analysing degradation and collapse in postbuckling composite aerospace structures. *Journal of Composite Materials* 43(26):3239–3263, 2009. doi: [10.1177/0021998309345294](https://doi.org/10.1177/0021998309345294).
- [20] C.G. Dávila and C. Bisagni. Fatigue life and damage tolerance of postbuckled composite stiffened structures with initial delamination. *Composite Structures*, 161:73–84, 2017. doi: [10.1016/j.compstruct.2016.11.033](https://doi.org/10.1016/j.compstruct.2016.11.033).
- [21] E. Pietropaoli and A. Riccio. On the robustness of finite element procedures based on Virtual Crack Closure Technique and fail release approach for delamination growth phenomena. Definition and assessment of a novel methodology. *Composites Science and Technology*, 70(8):1288–1300, 2010. doi: [10.1016/j.compscitech.2010.04.006](https://doi.org/10.1016/j.compscitech.2010.04.006).
- [22] E. Pietropaoli and A. Riccio. Formulation and assessment of an enhanced finite element procedure for the analysis of delamination growth phenomena in composite structures. *Composites Science and Technology*, 71(6):836–846, 2011. doi: [10.1016/j.compscitech.2011.01.026](https://doi.org/10.1016/j.compscitech.2011.01.026).
- [23] Y.P. Liu, G.Q. Li, and C.Y. Chen. Crack growth simulation for arbitrarily shaped cracks based on the virtual crack closure technique. *International Journal of Fracture*, 185:1–15, 2014. doi: [10.1007/s10704-012-9790-3](https://doi.org/10.1007/s10704-012-9790-3).
- [24] Y.P. Liu, C.Y. Chen, and G.Q. Li. A modified zigzag approach to approximate moving crack front with arbitrary shape. *Engineering Fracture Mechanics*, 78(2):234–251, 2011. doi: [10.1016/j.engfracmech.2010.08.007](https://doi.org/10.1016/j.engfracmech.2010.08.007).

- [25] A. Riccio, M. Damiano, A. Raimondo, G. di Felice, and A. Sellitto. A fast numerical procedure for the simulation of inter-laminar damage growth in stiffened composite panels. *Composite Structures*, 145:203–216, 2016. doi: [10.1016/j.compstruct.2016.02.081](https://doi.org/10.1016/j.compstruct.2016.02.081).
- [26] K.F. Nilsson, L.E. Asp, J.E. Alpmann, and L. Nystedt. Delamination buckling and growth for delaminations at different depths in a slender composite panel. *International Journal of Solids and Structures*, 38(17):3039–3071, 2001. doi: [10.1016/S0020-7683\(00\)00189-X](https://doi.org/10.1016/S0020-7683(00)00189-X).
- [27] R.A. Jurf and R.B. Pipes. Interlaminar fracture of composite materials. *Journal of Composite Materials*, 16(5):386–394, 1982. doi: [10.1177/002199838201600503](https://doi.org/10.1177/002199838201600503).
- [28] R.L. Ramkumar and J.D. Whitcomb. Characterisation of mode I and mixed-mode delamination growth in T300/5208 graphite/epoxy. In: W. Johnson (ed.), *Delamination and Debonding of Materials*, pages 315–335, ASTM, Philadelphia, 1985. doi: [10.1520/STP36312S](https://doi.org/10.1520/STP36312S).
- [29] S. Hashemi, A.J. Kinloch, and J.G. Williams. The effects of geometry, rate and temperature on mode I, mode II and mixed-mode I/II interlaminar fracture of carbon-fibre/poly(ether-ether-ketone) composites. *Journal of Composite Materials*, 24(9):918–956, 1990. doi: [10.1177/002199839002400902](https://doi.org/10.1177/002199839002400902).
- [30] S. Hashemi, A.J. Kinloch, and J.G. Williams. Mixed-mode fracture in fiber-polymer composite laminates. In: T. O'Brien (ed.) *Composite Materials: Fatigue and Fracture*, vol. 3, pages 143–168, ASTM, Philadelphia, 1991. doi: [10.1520/STP17717S](https://doi.org/10.1520/STP17717S).
- [31] C. Hwu, C.J. Kao, and L.E. Chang. Delamination fracture criteria for composite laminates. *Journal of Composite Materials*, 29(15):1962–1987, 1995. doi: [10.1177/002199839502901502](https://doi.org/10.1177/002199839502901502).
- [32] M.L. Benzeggagh and M. Kenane. Measurement of mixed-mode delamination fracture toughness of unidirectional glass/epoxy composites with mixed-mode bending apparatus. *Composites Science and Technology*, 56:439–449, 1996.
- [33] N.B. Adeyemi, K.N. Shivakumar, and V.S. Avva. Delamination fracture toughness of woven-fabric composites under mixed-mode loading. *AIAA Journal*, 37(4):517–520, 1999. doi: [10.2514/2.747](https://doi.org/10.2514/2.747).
- [34] J.R. Reeder. 3D mixed-mode delamination fracture criteria – an experimentalist’s perspective. In: *American Society for Composites 21st Annual Technical Conference*, document ID: 20060048260, Dearborn, USA, 2006.
- [35] R. Kruger. Virtual crack closure technique: History, approach, and applications. *Applied Mechanics Reviews*, 57(2):109–143, 2004. doi: [10.1115/1.1595677](https://doi.org/10.1115/1.1595677).
- [36] E.J. Barbero. *Finite Element Analysis of Composite Materials*, CRC Press, Boca Raton, 2014.
- [37] J.W. Hutchinson, M.E. Mear, and J.R. Rice. Crack paralleling an interface between dissimilar materials. *Journal of Applied Mechanics*, 54(4):828–832, 1987. doi: [10.1115/1.3173124](https://doi.org/10.1115/1.3173124).
- [38] M.A. Tashkinov. Modelling of fracture processes in laminate composite plates with embedded delamination. *Frattura ed Integrità Strutturale*, 11(39):248–262, 2017. doi: [10.3221/IGF-ESIS.39.23](https://doi.org/10.3221/IGF-ESIS.39.23).
- [39] A.B. Pereira and A.B. de Morais. Mode II interlaminar fracture of glass/epoxy multidirectional laminates. *Composites Part A: Applied Science and Manufacturing*, 35(2):265–272, 2004. doi: [10.1016/j.compositesa.2003.09.028](https://doi.org/10.1016/j.compositesa.2003.09.028).
- [40] A.B. Pereira and A.B. de Morais. Mode I interlaminar fracture of carbon/epoxy multidirectional laminates. *Composites Science and Technology*, 64(13-14):2261–2270, 2004. doi: [10.1016/j.compscitech.2004.03.001](https://doi.org/10.1016/j.compscitech.2004.03.001).